ORIGINAL ARTICLE

Study on the relationship between interface morphology and mechanical properties of explosive welded titanium/duplex stainless steel

Minjing Wang[1,3,4] · Jianian Hu[1,3,4] · Kebin Li[2,7] · Ning Luo[5] · Xiaojie Li[6] · Xiang Chen[1,3,4] · Zhen Chen[4]

Abstract

This study investigated the interface morphology and mechanical properties of titanium (TP 270C)/duplex stainless steel (SUS 821L1) near the lower limit of the explosive welding window. Seven samples with different welding parameters near the lower limit of the welding window were evaluated; the interface morphology was analyzed by optical microscopy (OM), scanning electron microscopy (SEM), computed tomography (CT), and smoothed particle hydrodynamics (SPH) simulation. The jet, interface shape, and temperature at the interface were obtained by simulation, demonstrating consistent interface shapes in the experimental results and simulation results. The energy produced at the interface was proportional to the element diffusion area. To assess the differences in mechanical properties between each sample, tensile shear tests and 90 bending tests were conducted. The results revealed that the sample with an average wavelength of 270 μm and an average amplitude of 62 μm had the best tensile properties. Furthermore, the maximum tensile strength was about 503 MP. In the bending test, samples with an average wavelength of 118–270 μm and an average amplitude of 20–62 μm showed no cracks at the welding interface after bending; however, cracks appeared at both large and no-wave interfaces.

Keywords Explosive welding · TP 270C/SUS 821L1 · Weldability window · Interface morphology · Mechanical properties

Nomenclature

V_C	Collision point velocity
β	Collision angle
V_P	Velocity of flyer plate
V_D	Detonation velocity
r	Loading ratio (mass of explosive per unit mass of flyer plate)
t_e	Explosive thickness
s	Stand-off distance
K	Gaseous polytropic index of the detonation products
L	Length
W	Width
H	Height
Z	Distance between TP207C and SUS 821L1 incisions
K	International unit of temperature, Kelvin

✉ Xiang Chen
  chenxiang@jhun.edu.cn

✉ Zhen Chen
  184139321@qq.com

1   State Key Laboratory of Precision Blasting, Jianghan University, Wuhan, People's Republic of China

2   State Key Laboratory of Explosion Science and Technology, Beijing Institute of Technology, Beijing, People's Republic of China

3   Hubei Province Key Laboratory of Engineering Blasting, Jianghan University, Wuhan, People's Republic of China

4   School of Digital Construction and Blasting Engineering, Jianghan University, Wuhan, People's Republic of China

5   State Key Laboratory for Geo-Mechanics and Deep Underground Engineering, School of Mechanics and Civil Engineering, China University of Mining and Technology, Xuzhou, China

6   State Key Laboratory of Structural Analysis, Optimization and CAE Software for Industrial Equipment, Dalian University of Technology, Dalian 116024, Liaoning, People's Republic of China

7   Key Laboratory of Impact and Safety Engineering, Ministry of Education, Ningbo University, Ningbo, People's Republic of China

Table 1 Mechanical properties of materials

Materials	Density (g/cm^3)	Yield strength (N/mm^2)	Tensile strength (N/mm^2)	Elongation (%)	Hardness (HB)
TP 270C	4.51	$\geq$ 165	270–410	$\geq$ 27	-
SUS 821L1	7.80	$\geq$ 400	$\geq$ 600	$\geq$ 25	$\leq$ 290
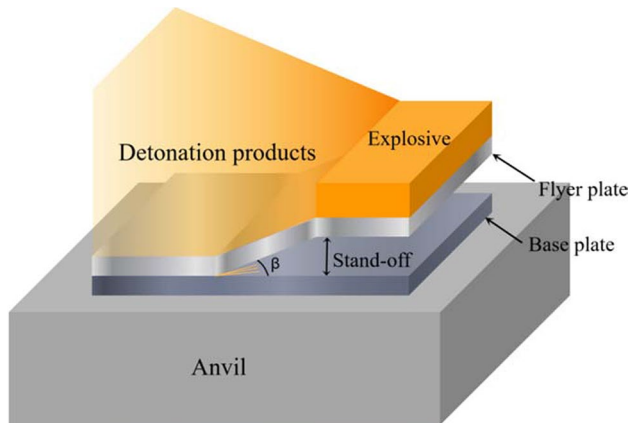
Fig. 1 Schematic of explosive welding

1 Introduction

Titanium is widely used in aerospace, petrochemical, medical, and other fields due to its high strength, good toughness, and excellent corrosion resistance [1]. SUS 821L1 is a new stainless steel material characterized by high strength, low cost, and good corrosion resistance [2]. At present, the welding methods to connect titanium and stainless steel include electron beam welding [3], laser welding [4, 5], friction welding [6, 7], and brazing welding [8]. However, these methods have limitations such as uneven heating of the weld seam or excessive residual stress, and cannot be effectively used for high-strength large-scale welding [9]. Explosive welding is a solid-state welding process with great potential for connecting different materials.

Explosive welding is achieved by controlling the energy released during the explosion process to form high-speed oblique collisions between plates, thereby achieving tight welding [10–12]. Wittman [13] and Deribas et al. [14] proposed an applicable concept for explosive welded windows. The concept takes into account the collision point velocity (V_C) and collision angle (β) in the horizontal direction. Superior welding results are obtained when the welding parameters are kept within the welding window. Wang et al. [15] determined the appropriate welding parameters within the weldability window and successfully welded a thick copper plate and a thick steel plate. Athar et al. [16] reported a superior welding effect with a wave interface obtained while respecting the explosive weldability window. Inao et al. [17] mentioned that the lower limit of the explosive weldability window can be used to improve the quality of explosive welding materials. Much research has been conducted on the influence of test parameters such as collision velocity and collision angle on welding quality. Akbari et al. [18] determined the calculation method of explosive "welded window" between CP-titanium and AISI 304 stainless steel. The experimental results showed that the wavelength and amplitude increased with the explosion load in the "welding window." Shi et al. [19] discussed the effect of the explosion thickness on the bonding quality of the explosion cladding 410S steel and Q345R steel. The samples with microwavy interfaces had minor interfacial deformation, fewer defects, and the highest bonded strength. Therefore, investigating the relationship between welding interface morphology and mechanical properties is of great significance.

Table 2 The experimental parameters for explosive welding

Sample	Thickness of explosive (mm)	Stand-off distance (mm)	Thickness of flyer plate (mm)	Thickness of base plate (mm)	Welding results
1	28	1.2	3	3	Welded
2	38	2	3	3	Welded
3	38	3	3	3	Welded
4	28	3.5	3	3	Welded
5	28	2.2	3	3	Welded
6	48	5	3	3	Welded
7	48	15	3	3	Welded

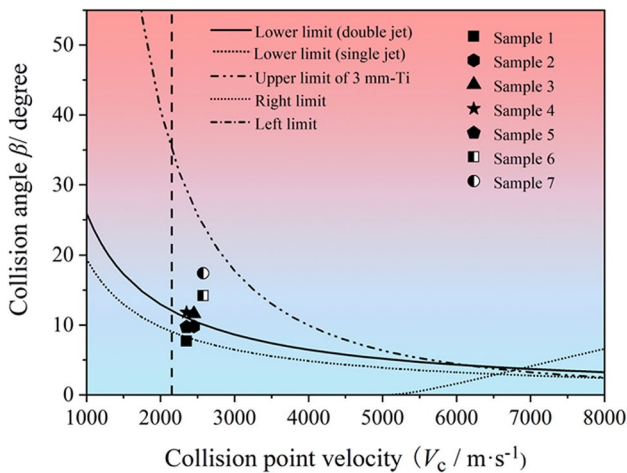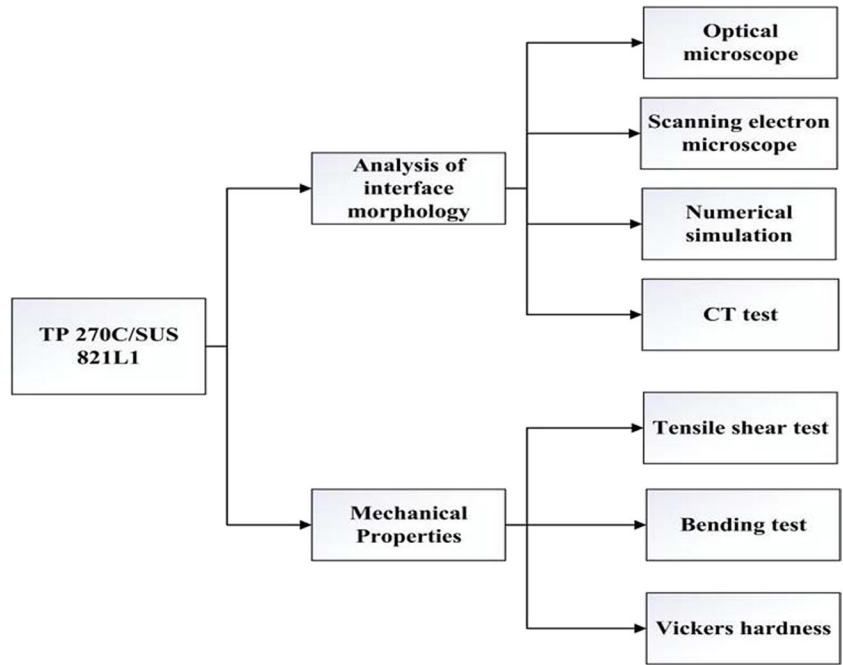**Fig. 2** Test flow chart

Fig. 3 The weldability window of TP 270C/SUS 821L1

This study is based on previous research describing the TP 270C/SUS 821L1 weldability window [20]. The parameters for welding were set to near the lower limit of the weldability window to explore the relationship between the interface morphology and mechanical properties, and the optimal parameters were determined by applying the artificial neural network concept [21]. Optical microscopy (OM), scanning electron microscopy (SEM), computed tomography (CT), and energy dispersion spectroscopy (EDS) were used to analyze the microstructure of the welding interface. The jet, interface morphology (including wave and vortex), and interface temperature during welding were studied by smoothed particle hydrodynamics (SPH) simulation. Tensile shear tests and bending tests were carried out to evaluate the mechanical properties.

Table 3 The calculated values of V_P, β

Sample	K	Explosive ratio, r	Detonation velocity, V_D (m/s)	Velocity of flyer, plate, V_P (m/s)	Collision angle, β
1	2.20	1.0	2350	316	7.7°
2	2.37	1.4	2450	419	9.8°
3	2.37	1.4	2450	495	11.6°
4	2.20	1.0	2350	483	11.8°
5	2.20	1.0	2350	397	9.7°
6	2.48	1.8	2575	637	14.2
7	2.48	1.8	2575	779	17.4
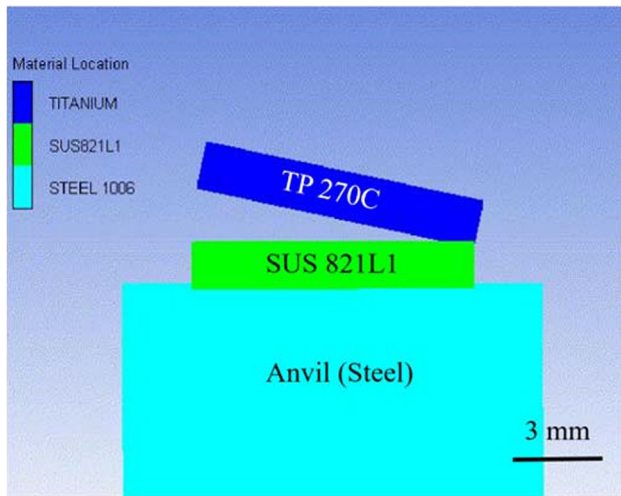
Fig. 4 Numerical simulation model

2 Materials and methods

2.1 Materials

JIS TP 270C and SUS 821L1(ferrite and austenite approximately 50% each) of sizes 200 mm × 100 mm × 3 mm (length × width × height) and low carbon steel anvil substrate of 260 mm × 140 mm × 60 mm (length × width × height) were used in this study. The chemical compositions of TP 270C and SUS 821L1 are provided in the reference [2], and the mechanical properties of the materials are shown in Table 1. The primary

explosive used in this experiment is ANFO-A (ammonium nitrate and fuel oil base), with a density of about 530 kg/m^3. The schematic diagram of explosive welding is illustrated in Fig. 1, and the experimental parameters, such as the distance between the flyer plate and the base plate, are shown in Table 2. In addition, the test method used in this study is displayed in Fig. 2.

2.2 Welding parameters

The weldability window for TP 270C/SUS 821L1 is shown in Fig. 3. As described in previous research [20], the single jet limit was titanium jet occurs and the double jet limit was titanium jet and stainless steel jet both occurs during explosive welding. Based on the results of previous studies [20, 22], the welding parameters were set as follows. Sample 1 was located below the single jet limit so that no jet was generated in the welding process, whereas samples 2 and 5 were located above the single jet limit and below the double jet limit. In the welding process, a single jet was generated only on the titanium side. Samples 3 and 4 were located above the double jet limit (wavy interface limit), yielding a microwave-shaped interface. Samples 6 and 7 were located at a certain distance above the double jet limit, forming large waves at the interface. Moreover, the collision angle of sample 7 was larger than that of sample 6, so the interface wave generated by sample 7 was larger than that of sample 6. The welding parameters are shown in Fig. 3 and Table 3. The relationship between the velocity of the flyer plate (V_P) in the vertical direction and the collision angle (β) can be expressed by the following formula [23]:

Fig. 5 Schematic diagram of the tensile shear test sample (**a**). Schematic diagram of the three-point face bending test sample (**b** and **c**)
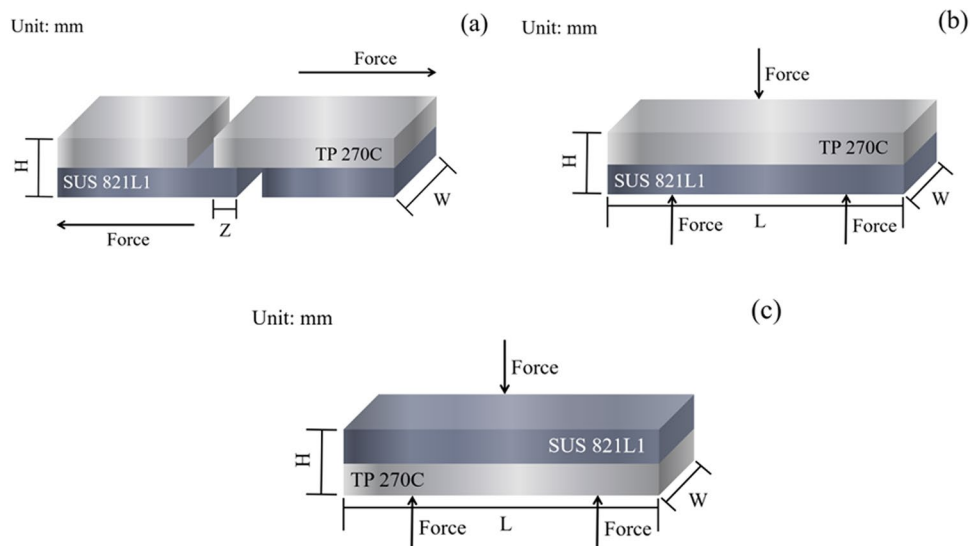
Fig. 6 Optical analysis and numerical simulation of the interface: **a** sample 1; **b** sample 2; **c** sample 3; **d** sample 4; **e** sample 5; **f** sample 6; **g** sample 7
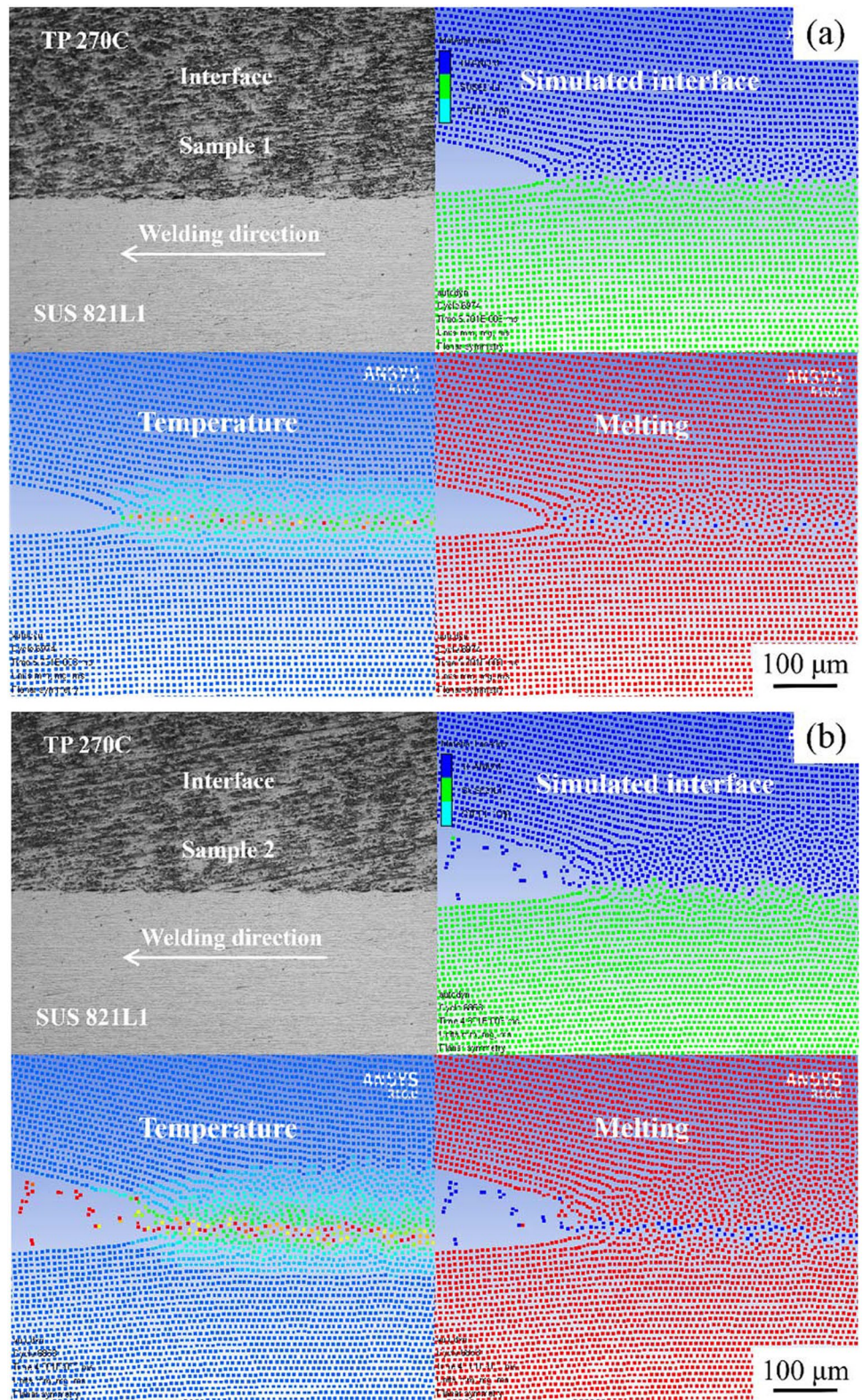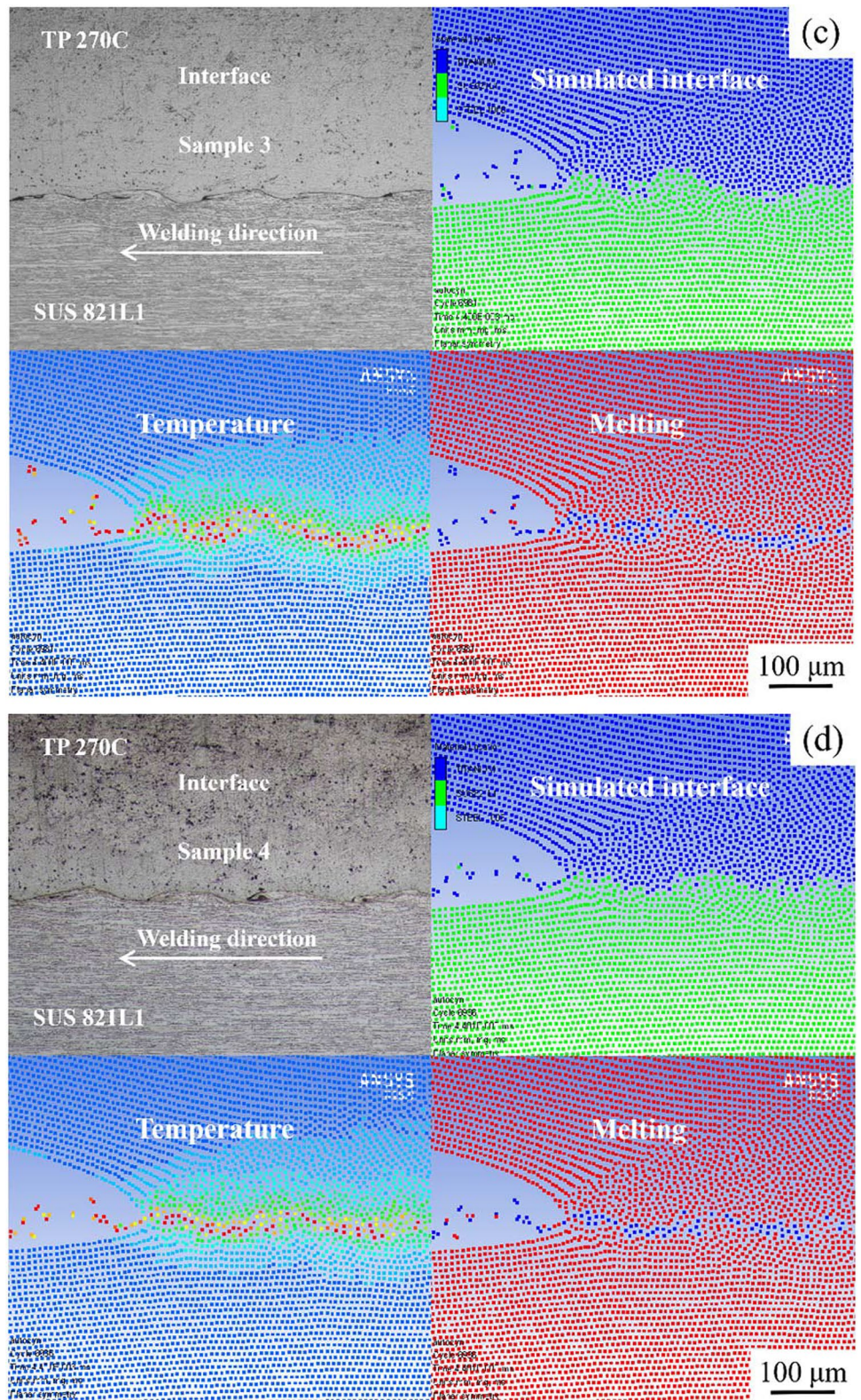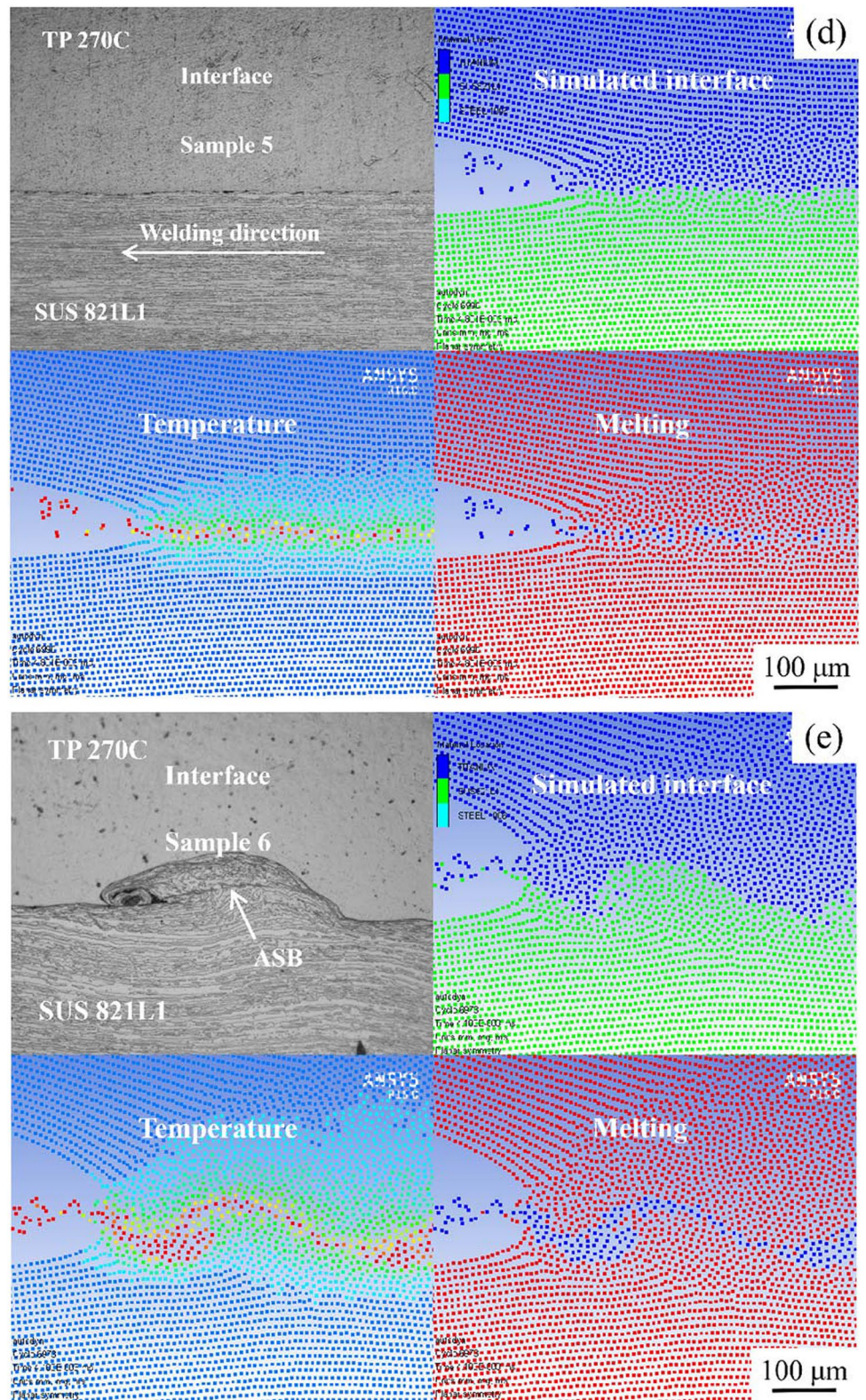
Fig. 6 (continued)

Fig. 6 (continued)

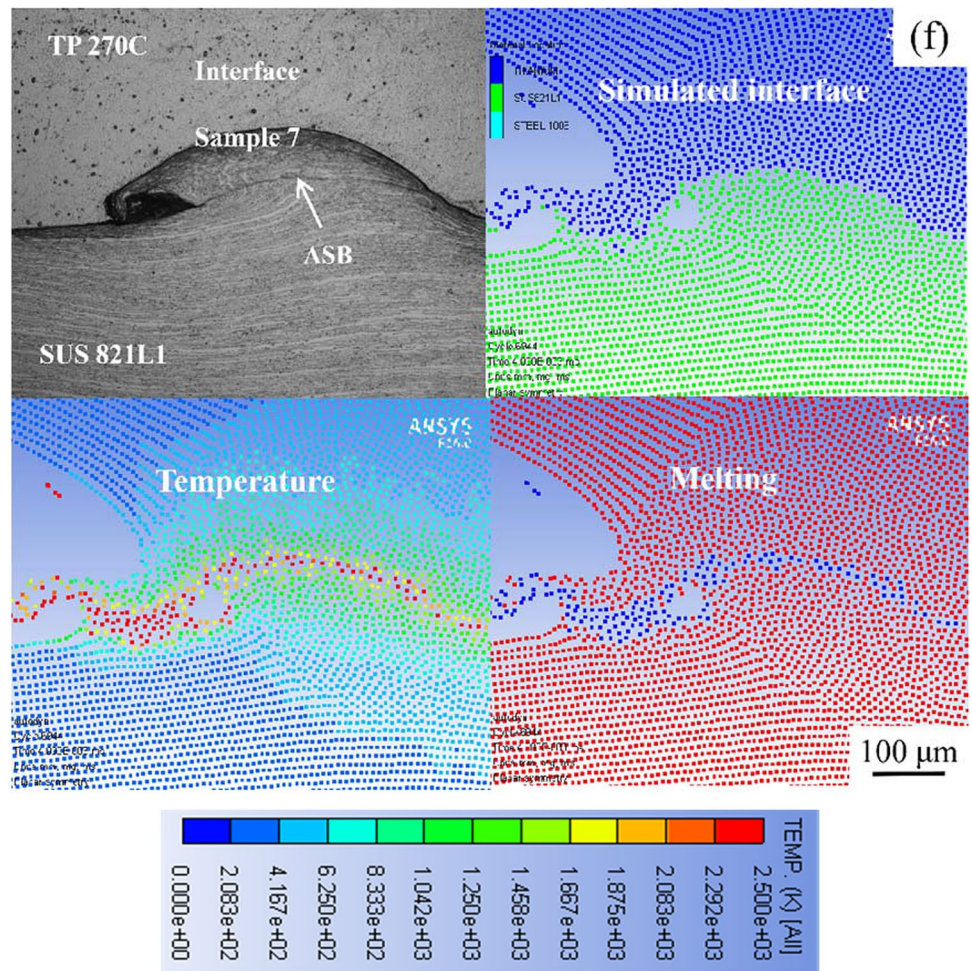**Fig. 6** (continued)

$$V_P = 2V_D \sin\frac{\beta}{2} \tag{1}$$

where V_D is the detonation velocity of the explosive. The collision angle β is calculated by the equation in reference [24].

$$\beta = (\sqrt{\frac{K+1}{K-1}} - 1)\frac{\pi}{2}\frac{r}{r + 2.71 + \frac{0.184t_e}{s}} \tag{2}$$

where r represents the loading ratio (mass of explosive per unit mass of flyer plate), t_e represents the explosive thickness, s represents the stand-off distance, and K is the gaseous polytropic index of the detonation products. Parameters K and V_D were obtained from references [25, 26], as shown in Table 3.

2.3 Numerical simulations

The commercial code ANSYS/Autodyn was used to simulate explosive welding. Compared with other methods, the smooth particle fluid dynamics (SPH) method is more suitable for the simulation of interface characteristics of explosive welding [27]. Therefore, the SPH method was used to simulate the welding process, as shown in Fig. 4. The size of the titanium and stainless steel plates was 20 mm (length) × 3 mm (height), with a particle size of 10 μm. The size of the anvil was 60 mm (length) × 30 mm (height), with a particle size of 100 μm. The initial velocity and collision angle in the simulation use the data in Table 3. Necessary physical parameters and EOS parameters were obtained from references [2, 20].

Fig. 7 Scanning electron microscopy images and EDS analysis results: **a** and **b** sample 1; **c** and d sample 4; **e** and **f** sample 6
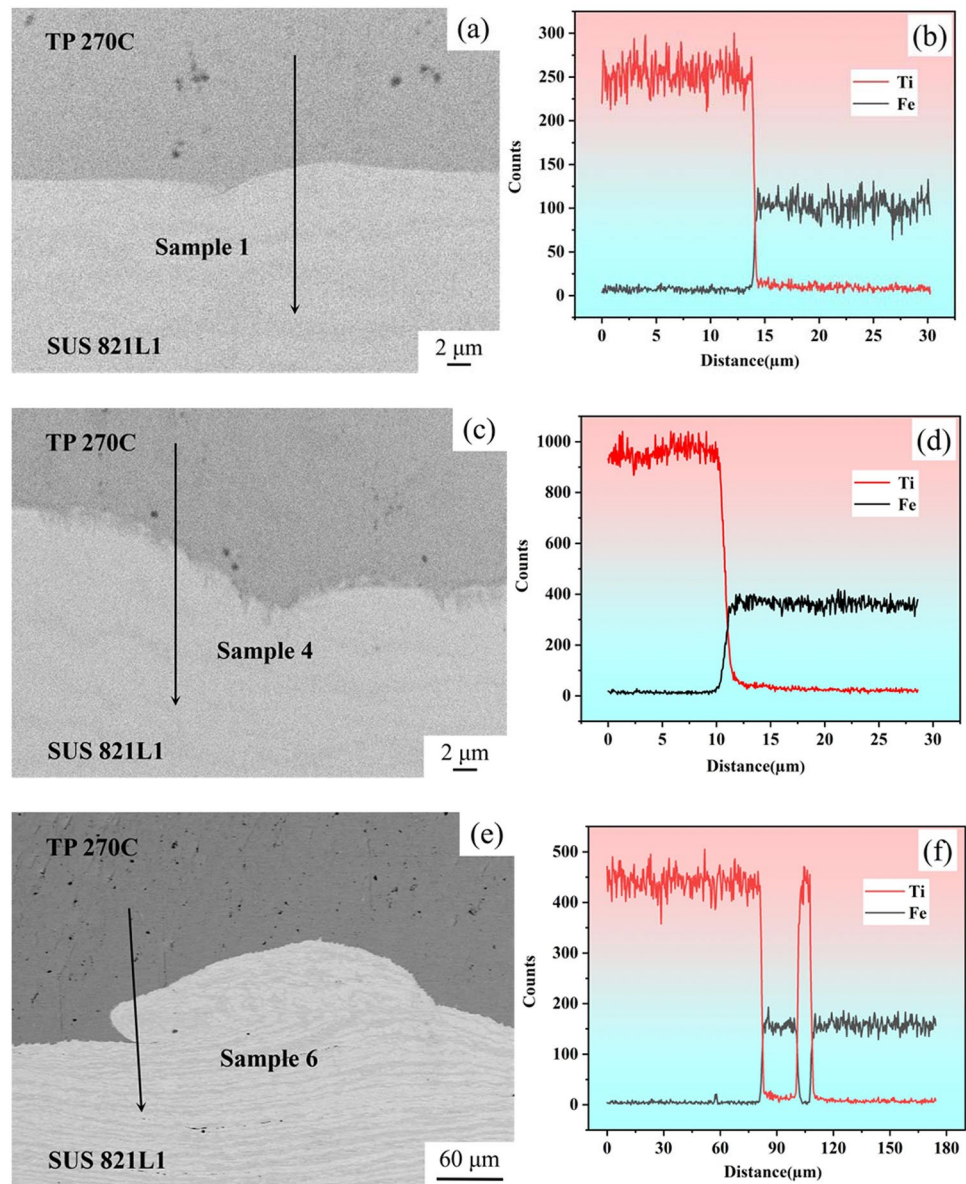
2.4 Mechanical properties

Mechanical properties were tested by the tensile shear test, bending test, and the Vickers hardness test. All three tests were performed at room temperature with a humidity of 50% [28]. The tensile shear test sample was cut along the welding direction, with a reserved incision size of 5 mm × 10 mm × 6 mm (length × width × height). The loading speed of the test machine was set to 1 mm/min. The schematic diagram of the tensile test sample is shown in Fig. 5a. The bending test sample had a size of

200 mm × 10 mm × 6 mm (length × width × height). Samples were bent on both sides (TP 270C, SUS 821L1), as shown in Fig. 5b and c.

3 Results and discussion

3.1 Analysis of interface morphology

The samples were polished and etched. The etching solution consisted of HF (3 mL), HNO_3 (6 mL), and H_2O
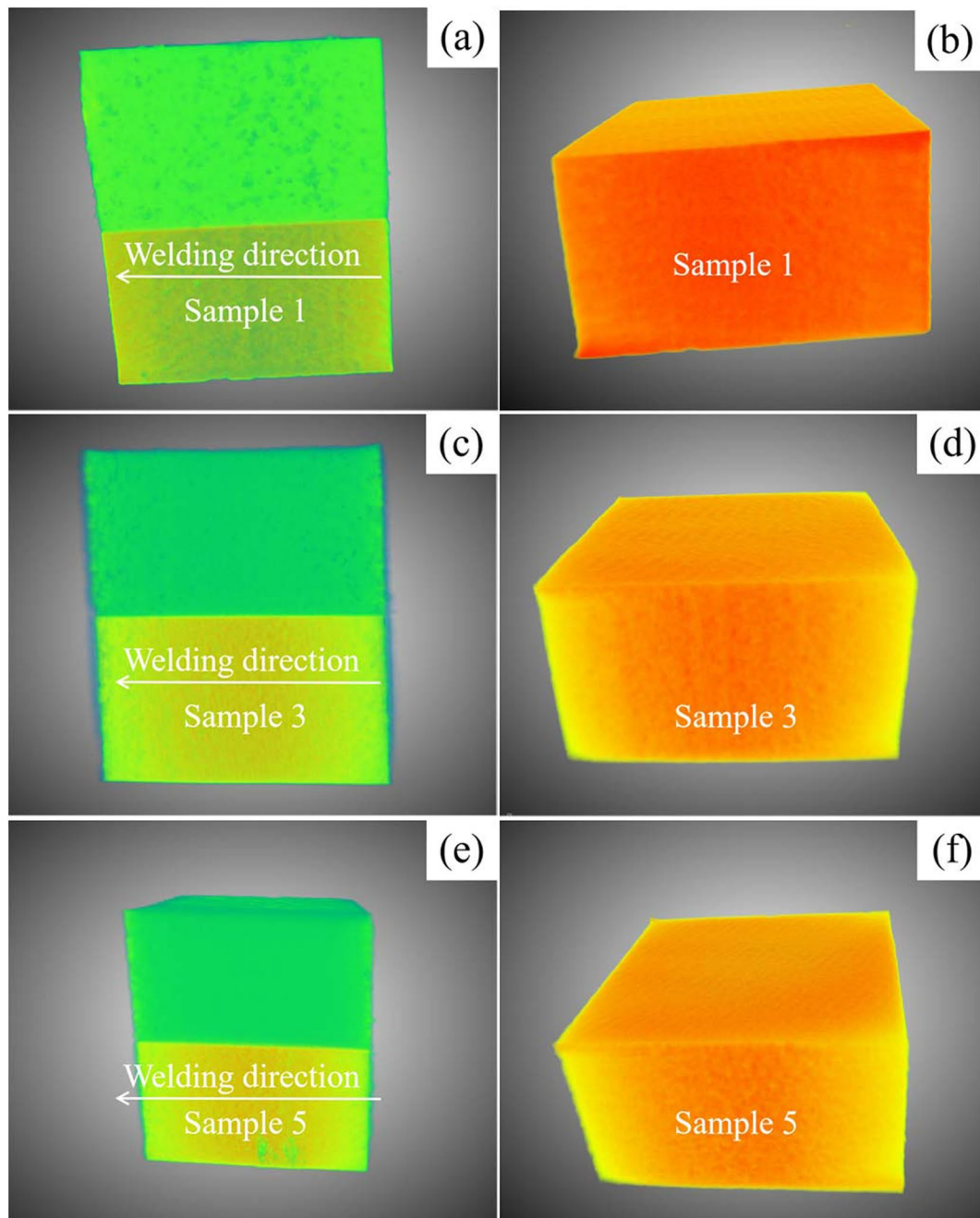
Fig. 8 Overall 3D diagram of SUS 821L1 and separation diagram: **a** and **b** sample 1; **c** and **d** sample 3; **e** and **f** sample 5; **g** and h sample 6; **i** and **j** sample 7

(91 mL) solutions. Optical microscopy was used to analyze the samples, and the interface obtained by welding and the simulation results are shown in Fig. 6. As displayed in Fig. 6a, sample 1 formed a nearly straight interface. The simulation results showed that sample 1 generated no jet in the welding process and did not form a continuous melting area due to the insufficient kinetic energy of the flyer plate. As displayed in Fig. 6b and e,
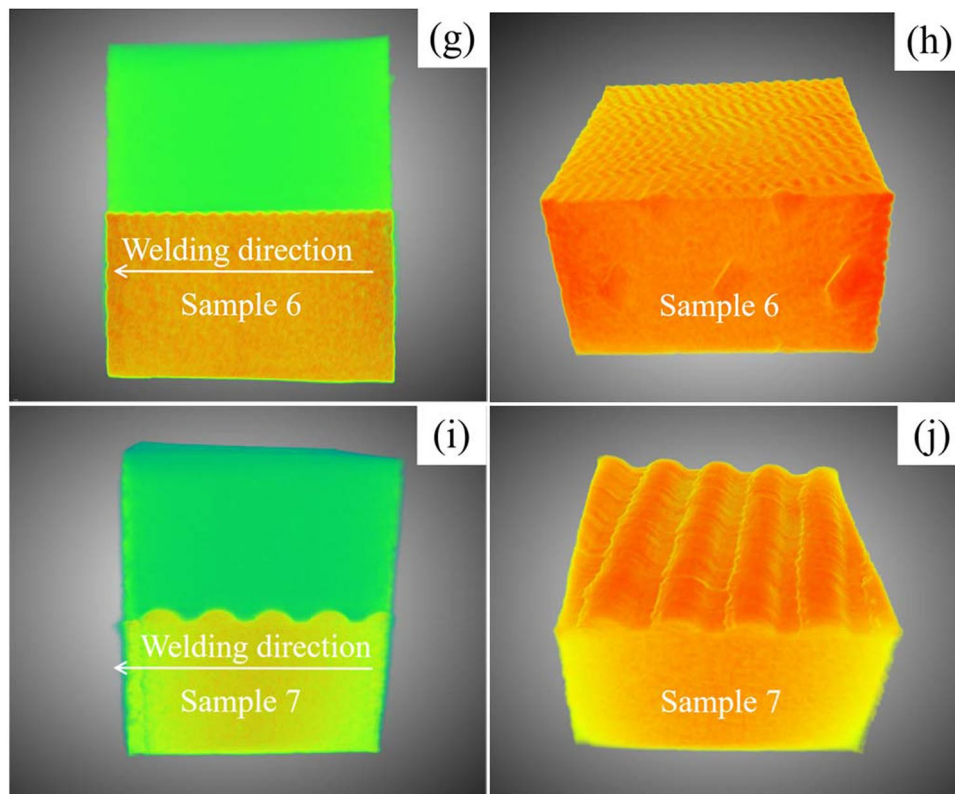
Fig. 8 (continued)

higher collision velocity and collision angle were produced in samples 2 and 5, producing a weak jet with no wavy interface and a continuous melting zone. Saresoja et al. also demonstrated that melting was a prerequisite for jet formation [29] using atomic simulation. In Fig. 6c, d, f, and g, samples 3, 4, 6, and 7 clearly showed a wavy interface with periodic changes at the welding interface, which was also the most significant feature in explosive welding [30]. Some studies also reported that the welding interface changed from a straight interface to a wavy interface as the explosives were increased [31]. The numerical simulation results verified the validity of the welding parameters determined by the window theory and were consistent with experimental results. Although the overall wavelength and amplitude of samples 3, 4, 6, and 7 were stable, the microscopic morphology of the vortex region of each wave was slightly different. The

average wavelength of the welding interface of samples 3 and 4 were 118 μm and 125 μm, and the average amplitudes were 20 μm and 22 μm, respectively. The average wavelength of the welding interface of samples 6 and 7 was 270 μm and 691 μm, and the average amplitudes were 62 μm and 190 μm, respectively. An obvious adiabatic shear band (ASB) was observed in samples 6 and 7, which represented one of the mechanisms of material failure caused by high strain rates in explosive welding and other processes [32].

The simulation results of the temperature field showed that the molten particles were concentrated in the vortex region, and a few were distributed along the entire length of the interface in the form of discrete points. The melting of the sample interface below the single and double jet limits (wavy limit) of the welding window was significantly less than that above the double jet limits (wavy limit).

Table 4 The results of the tensile shear test

Sample	1–1	1–2	1–3	2–1	2–2	2–3	3–1	3–2	3–3	4–1	4–2	4–3	5–1	5–2	5–3	6–1	6–2	6–3	7–1	7–2	7–3
Measured shear strength (MPa)	160	98	124	204	215	221	241	252	236	263	247	251	206	240	207	460	463	503	462	416	438

Green particles represented the base metal heat-affected zone near the interface, with a temperature range of about 1000–1450 K. In particular, the average simulated thickness of the heat-affected zone on the side of samples 6 and 7 reached 105 μm and 172 μm. The interface reached a significantly higher temperature than the melting point of the metal, exceeding 2500 K. In the von Mises stress cloud map, the region with Mises stress of 0 indicated the melting region and samples with large collision point velocity and collision angle showed a larger melting region. These findings are attributed to the oblique impact, strong plastic deformation, shear, friction, and agitation between the two materials, leading to a rapid increase in temperature at the interface [33]. High temperature promotes interatomic diffusion, forming different degrees of element diffusion at the interface.

3.2 Element diffusion of the interface in SEM

In order to study the diffusion of elements at the welding interface, element line analysis was carried out by energy dispersive spectroscopy (EDS). The EDS results are shown in Fig. 6. The black line in Fig. 5 indicates the EDS scanning line. The EDS results showed that the diffusion zone of elements in sample 1 was 0.4 μm, while that of sample 4 was 1.6 μm, and that in sample 6 was 4.7–6.4 μm. This is due to the dissipation of kinetic energy at the welding interface being accompanied by a rapid temperature rise in the bonding zone, resulting in the mutual diffusion of titanium and iron elements [34]. According to the simulation results of temperature at the interface in Fig. 7, the interface temperature was proportionate to the element diffusion area.

3.2.1 CT test

The CT test was performed to further observe the microstructure characteristics of the samples on the three-dimensional scale. The overall 3D picture of the sample and the 3D picture of the stainless steel side are shown in Fig. 8. Figure 8a, b, e, and f show a macroscopic perspective of the interface, which shows a flat surface with no wavy features between the titanium and stainless steel plates. In Fig. 8c and d, small wavy features can barely be observed at the interface from the macroscopic picture, and light wavy traces can be observed from the 3d drawing of stainless steel. In Fig. 8g and h, the interface shows an obvious wavy structure, with more regular and orderly. In Fig. 8i and j, the wavelength and amplitude of the interface are larger, and the wavy traces are more obvious. Figure 8h shows that the interface waves are not constant all the time.
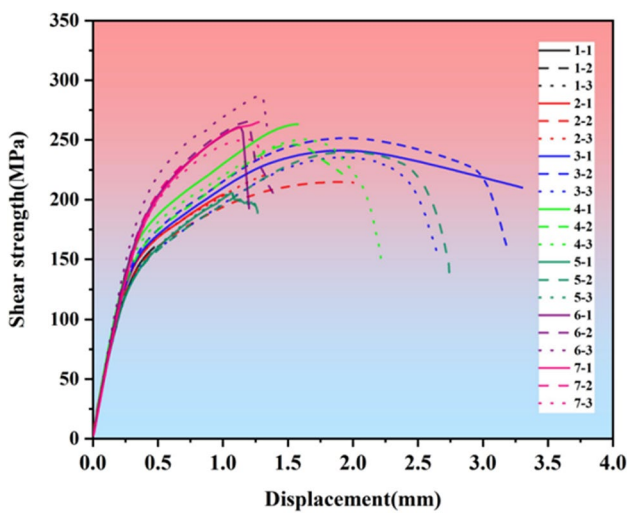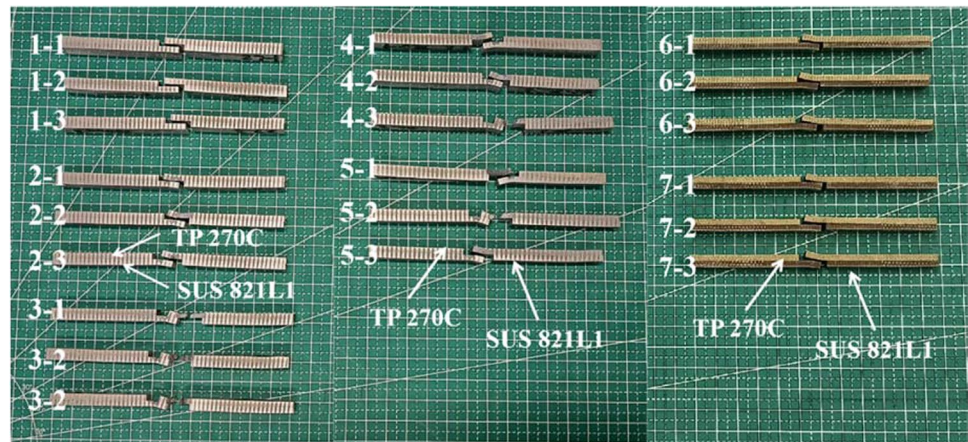
Fig. 9 Samples after stretching

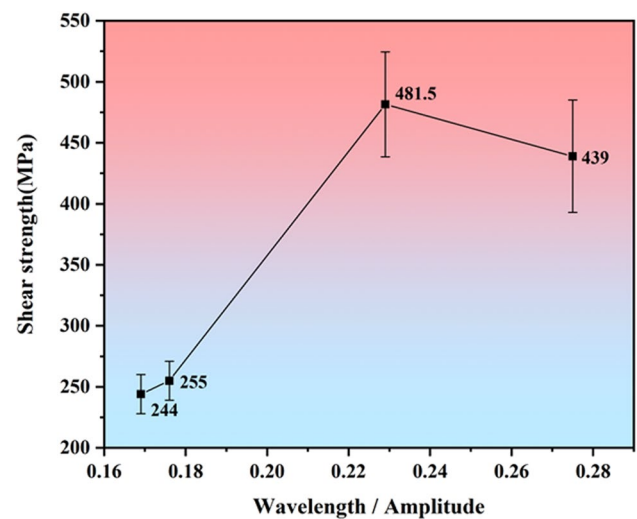**Fig. 10** Tensile curves

**Fig. 11** Tensile shear curves

3.3 Mechanical properties

3.3.1 Tensile shear test

In order to evaluate the welding strength of the welded plates [35, 36], a tensile shear test was conducted. The experimental parameters and results are shown in Table 4. Figure 9 illustrates the sample after the tensile test, and the tensile curve is shown in Fig. 10. The tensile strength of the samples ranked from small to large was sample 1 (98–160 MPa, no jet), samples 2, 5 (204–221 MPa, 206–240 MPa, no wavy interface), samples 3, 4 (236–252 MPa, 247–263 MPa, microwavy interface), sample 7 (416–462 MPa, large wavy interface), and sample 6 (460–503 MPa, small wavy interface). The tensile strength of the small wavy interface samples was 273% and 116% higher than the no-jet and no-wave samples, 88% higher than the microwave samples, and 10% higher than the large wave samples. The relationship between tensile strength and wavelength/amplitude is shown in Fig. 11. The experimental results show that excessively large or small interface waves are detrimental to the bonding strength of the interface, with moderate-sized waves being optimal.

Fig. 12 Fracture analysis on the titanium and stainless steel sides: **a** and **b** sample 1; **c** and **d** sample 2; **e** and **f** sample 3; **g** and **h** sample 4; **i** and **j** sample 5; **k** and **l** sample 6; **m** and **n** sample 7
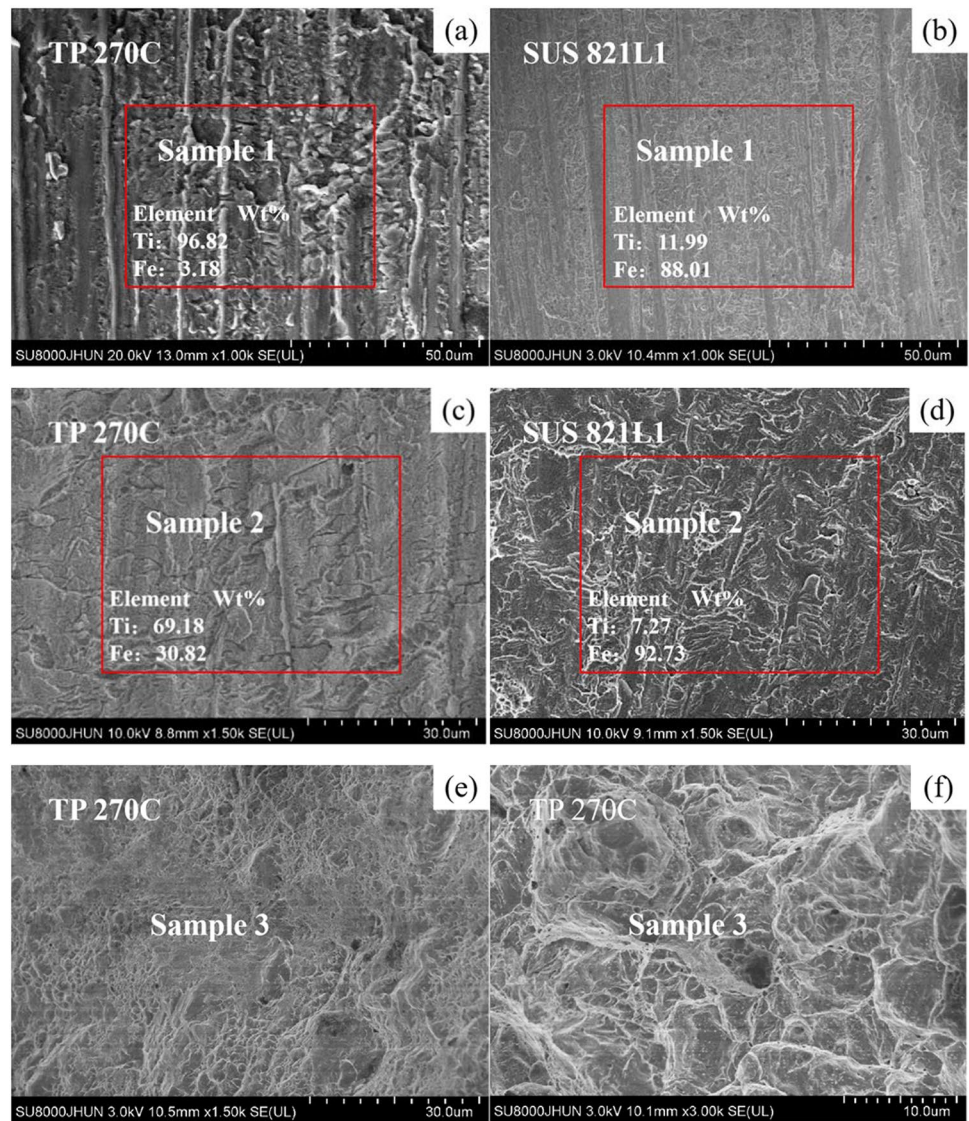
In order to determine the accurate fracture location and characteristics of the samples, the fracture surface was analyzed from a macroscopic and microscopic perspective, as shown in Figs. 9 and 12. Samples 1 and 2 were fractured at the welding interface, as shown in Fig. 9. According to the EDS analysis, the TP 270C elements in samples 1 and 2 contained 96.85 wt% and 69.18 wt% Ti elements, respectively. In comparison, the SUS 821L1 side contained Fe elements of 88.01 wt% and 92.73wt%, respectively. The results indicated that the fracture of samples 1 and 2 occurred at the welding interface, with the fracture surface showing the cleavage features and the groove. The fracture was mainly brittle, which was consistent with the tensile curve in Fig. 10 suggesting that the failure was

Fig. 12 (continued)
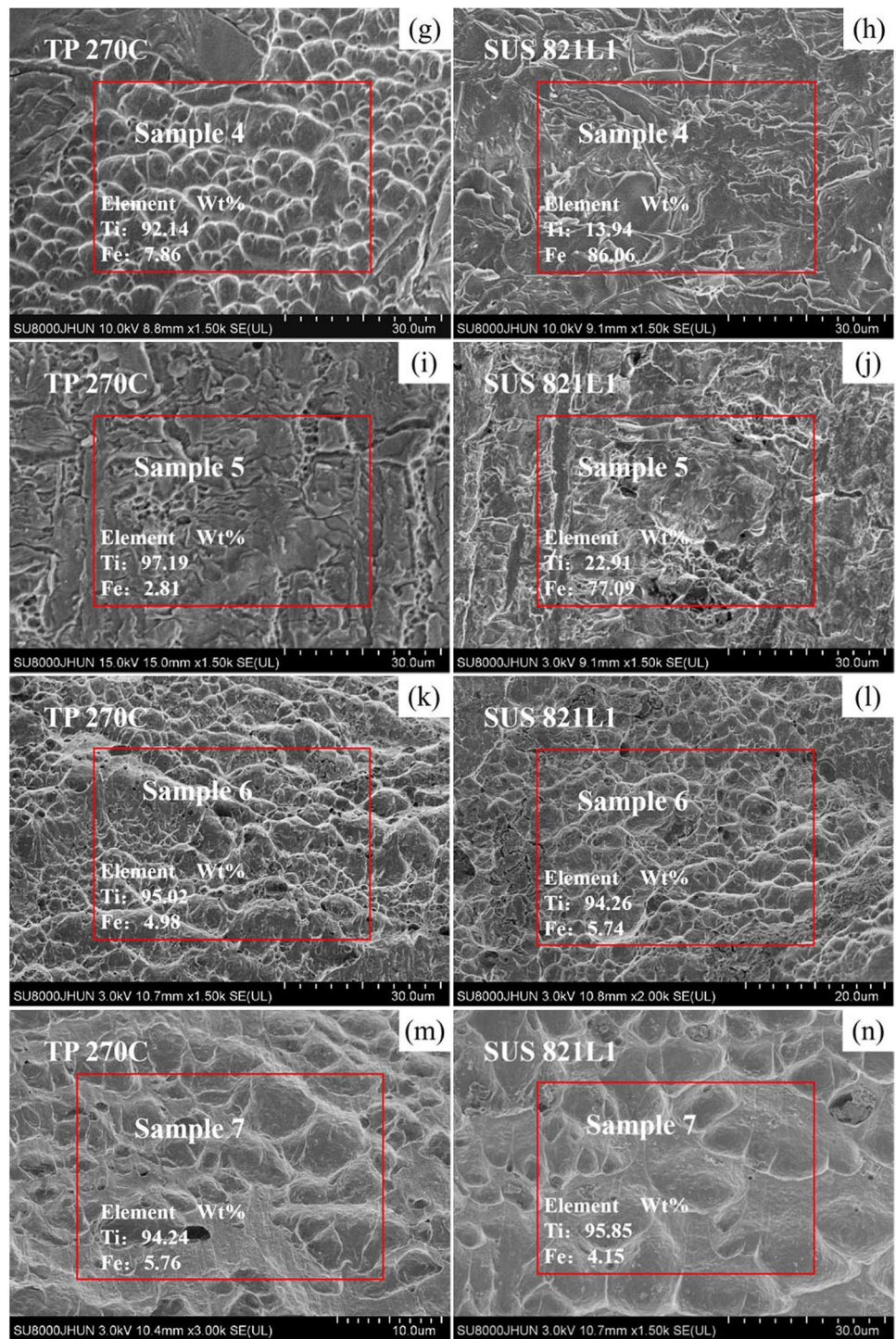
caused by sliding shear. Sample 3 was fractured at the titanium side as displayed in Fig. 9. According to Fig. 12, the fracture of sample 3 was full of dimples and pores; the fracture exhibited characteristics of ductile fracture. The tensile shear curve of sample 3 was similar to the

tensile curve of TP 270C and showed excellent resilience. Samples 4 and 5 were fractured at the titanium side, while samples 6 and 7 were fractured at the welding interface, as displayed in Fig. 9. According to the EDS analysis, the TP 270C side of samples 6 and 7 contained Ti elements
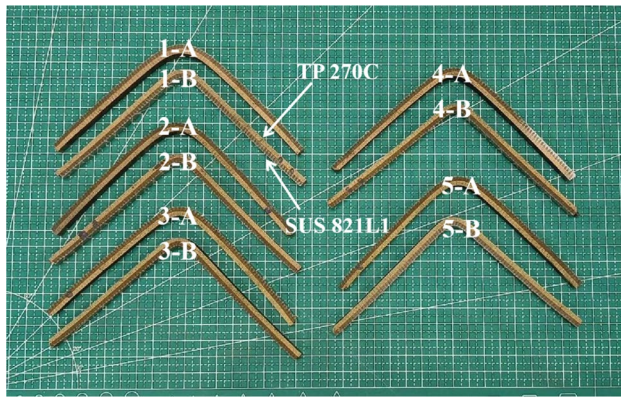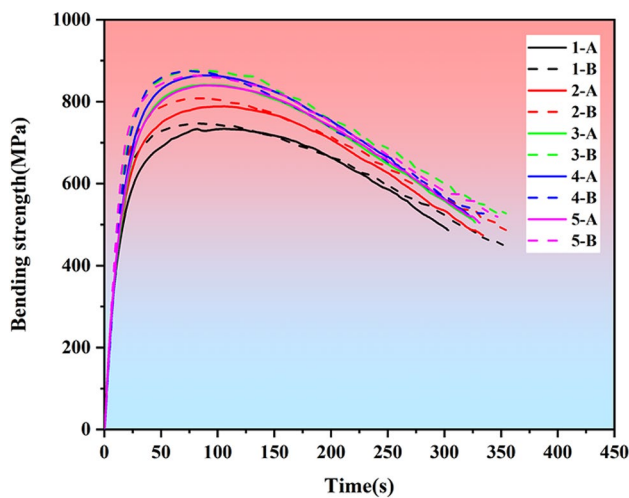
Fig. 13 Samples after bending


Fig. 14 Bending curves

of 95.02 wt% and 94.24 wt%. Instead, the SUS 821L1 side contained 5.74 wt% and 4.15 wt% Fe elements, indicating that the fracture of samples 6 and 7 occurred on the titanium side. The curve was suggestive of a brittle fracture,

mainly showing quasi-cleavage morphology, which may be related to the adiabatic shear band generated on the titanium side near the interface [2]. Therefore, different welding parameters produce different fracture results and fracture morphology.

3.3.2 Bending test

In order to evaluate the deformation resistance of the explosive welded parts [37, 38], a three-point bending test was adopted for the samples, and 90° bending was measured. For samples 1–5, A and B (TP 270C, SUS 821L1) were bent on both sides, while the bending results and test data of samples 6 and 7 were referred to in the literature [22]. The results are shown in Fig. 13 and Fig. 14. The macroscopic results showed no macroscopic separation and fracture after bending, with a larger bending curvature towards the B-plane. Optical microscopy analysis was performed on samples 1, 3, and 5 to further explore whether there are cracks in the welding interface after bending toward the B-plane. In Fig. 15a, cracks appeared on the interface, while in Fig. 15b and c, no cracks were observed on the interface. Moreover, no crack was observed at the interface of sample 6, while cracks were found at the interface of sample 7. This disparity indicated that the small wavy interface had strong resistance to plastic deformation [23]. In addition, the bending strength toward B was generally higher than that toward A, and the bending strength of samples 3 and 4 was higher than that of samples 1, 2, and 5. This difference can be attributed to the stronger work hardening (the flyer plate velocity of samples 3 and 4 was higher than samples 1, 2, and 5). The experimental results showed that the samples placed below the single jet line of the weldability window were prone to cracks, and the samples with excessively large interface waves also exhibited cracks after bending. However, the interfaces with microwave and small wavy shapes demonstrated good bending resistance.

Fig. 15 Bending results: **a** sample 1; **b** sample 3; **c** sample 5; **d** sample 6[22]; **e** sample 7 [22]
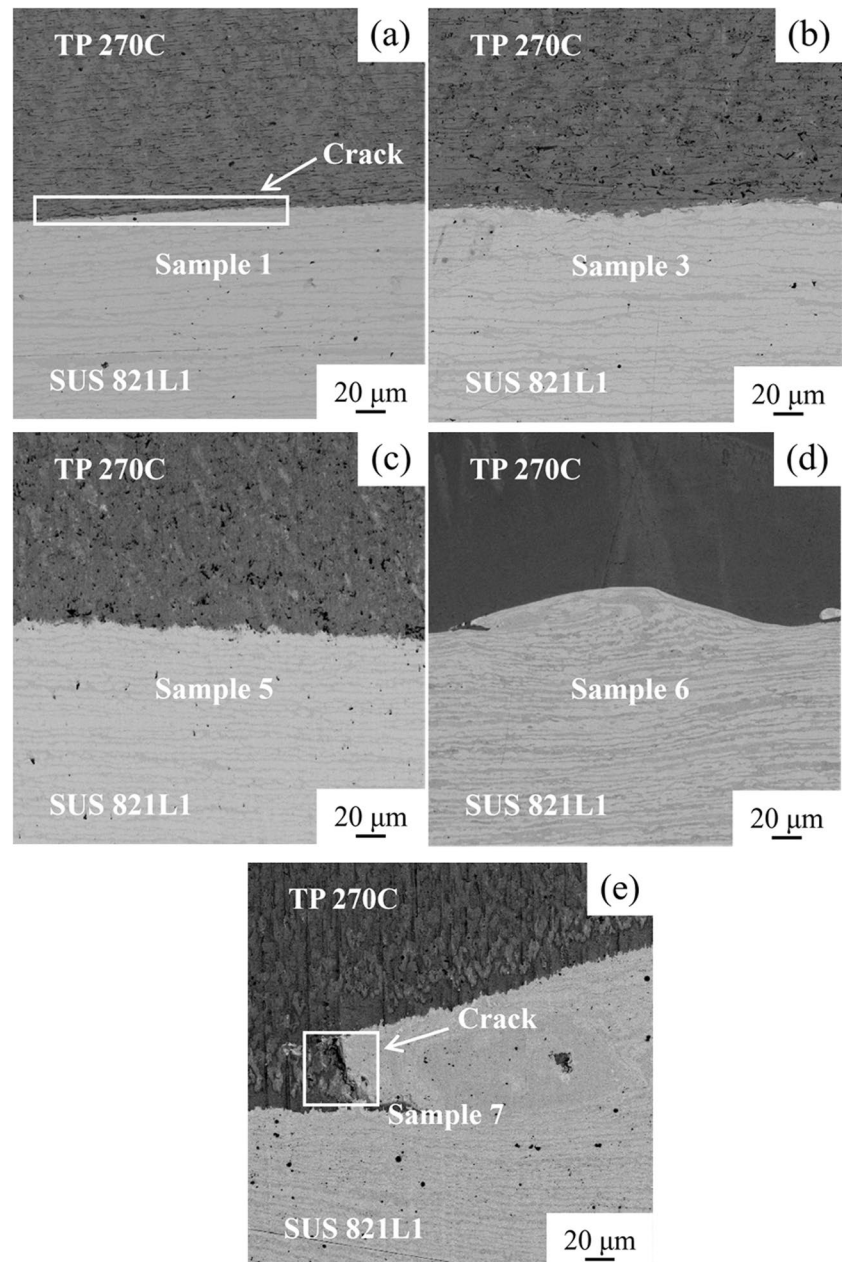
3.3.3 The Vickers hardness

This study used a microhardness testing machine for hardness testing, with a load of 0.2 kg and a residence time of 15 s. The results are displayed in Fig. 16. The microhardness value was highest near the weld interface of the sample, and decreased gradually as the distance from the weld interface was increased. In addition, the hardness value near the small wave interface (sample 6) was greater than the microwave interface and the no-wave interface. This was mainly due to the large plastic deformation of the small wave interface. Similar results were observed by Athar et al. [39] and Huang et al. [40].
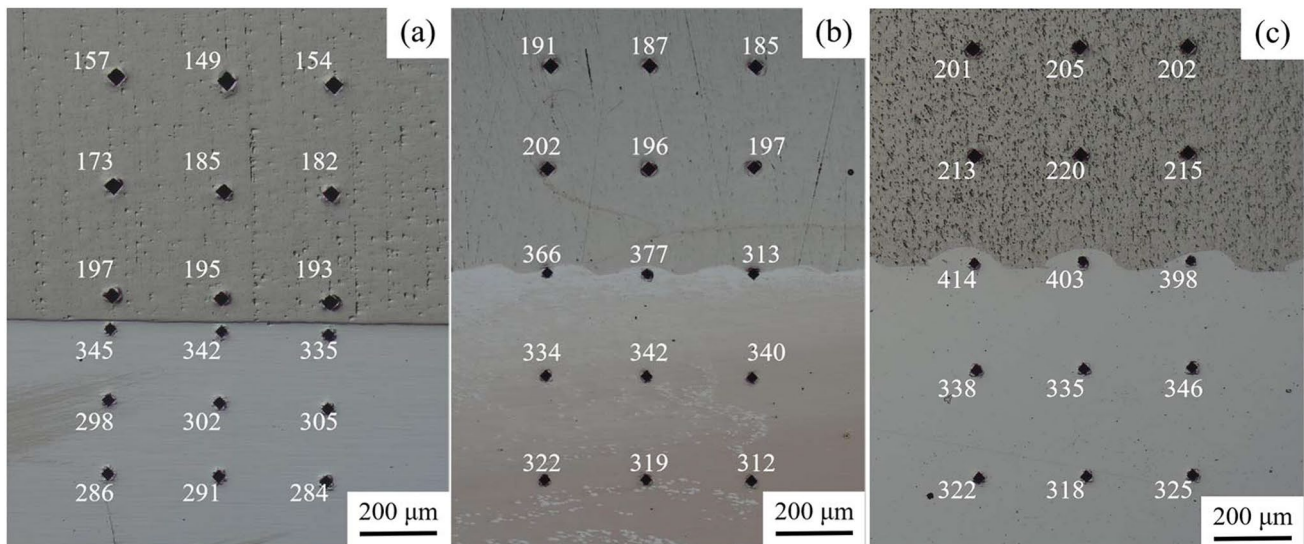
Fig. 16 The Vickers hardness test results: **a** sample 1; **b** sample 4; **c** sample 6

4 Conclusions

In this study, seven TP 270C/SUS 821L1 plates with different welding parameters near the lower limit of the weldability window were successfully fabricated by explosive welding. The relationship between the interface morphology and mechanical properties of explosive welding was studied. The following conclusions can be drawn.

1. The results of the metallographic experiment and simulation showed that no jet was generated in the welding process of sample 1. In the welding process of samples 2 and 5, only the titanium side produced a jet, while no jet was produced on the stainless steel side. Samples 3 and 4 produced a microwave interface with an average wavelength of 118 μm and 125 μm and an average amplitude of 20 μm and 22 μm, respectively. In contrast, samples 6 and 7 produced large wave interfaces, with an average wavelength of 270 μm and 691 μm and an average amplitude of 62 μm and 190 μm, respectively. However, sample 7 produced a larger interface wave than sample 6. The experimental and simulation results were consistent with the design.
2. The results of EDS and CT analyses showed an element diffusion zone of 0.4 μm in sample 1, 1.6 μm in sample 4, and 4.7–6.4 μm in sample 6. Higher collision point velocity and collision angle resulted in a larger amount of energy generated in the welding process, a higher interface temperature, a larger element diffusion area, and a more regular wavy structure.
3. The results of the tensile shear test and bending test showed that the welding interface with an average wavelength of 270 μm and an average amplitude of 62 μm has the best tensile shear performance. Furthermore, the maximum tensile shear strength was about 503 MP; compared with other samples, the tensile shear performance was improved by 10 to 273%. With an average wavelength of 118–270 μm and an average amplitude of 20–62 μm, no crack was observed in the welding interface after bending. In contrast, cracks occurred in both large and microwavy interfaces. The microhardness value was highest near the weld interface of the sample.

Data availability Not applicable.

Code availability Not applicable.

Declarations

Ethics approval Not applicable.

Consent to participate All authors have approved to participate.

Consent for publication The manuscript is approved by all authors for publication.

Conflict of interest The authors declare no competing interests.

References

1. Pushp P, Dasharath S, Arati C (2022) Classification and applications of titanium and its alloys. Mater Today Proc 54:537–542. https://doi.org/10.1016/j.matpr.2022.01.008

2. Chen X, Inao D, Tanaka S, Li X, Bataev I, Hokamoto K (2021) Comparison of explosive welding of pure titanium/SUS 304 austenitic stainless steel and pure titanium/SUS 821L1 duplex stainless steel. Trans Nonferrous Met Soc China 31:2687–2702. https://doi.org/10.1016/S1003-6326(21)65685-6

3. Kar J, Roy SK, Roy GG (2016) Effect of beam oscillation on electron beam welding of copper with AISI-304 stainless steel. J Mater Process Technol 233:174–185. https://doi.org/10.1016/j.jmatprotec.2016.03.001

4. Jiang D, Alsagri AS, Akbari M, Afrand M, Alrobaian A (2019) Numerical and experimental studies on the effect of varied beam diameter, average power and pulse energy in Nd: YAG laser welding of Ti6Al4V. Infrared Phys Technol 101:180–188. https://doi.org/10.1016/j.infrared.2019.06.006

5. Heydari H, Akbari M (2020) Investigating the effect of process parameters on the temperature field and mechanical properties in pulsed laser welding of Ti6Al4V alloy sheet using response surface methodology. Infrared Phys Technol 106:103267. https://doi.org/10.1016/j.infrared.2020.103267

6. Asmael M, Safaei B, Kalaf O, Zeeshan Q, Aldakheel F, Nasir T, Yang Z (2022) Recent developments in tensile properties of friction welding of carbon fiber-reinforced composite: a review. Nanotechnol Rev 11(1):1408–1436. https://doi.org/10.1515/ntrev-2022-0083

7. Adin MŞ, Okumuş M (2022) Investigation of microstructural and mechanical properties of dissimilar metal weld between AISI 420 and AISI 1018 STEELS. Arab J Sci Eng 47:8341–8350. https://doi.org/10.1007/s13369-021-06243-w

8. Slobodyan M (2022) Dissimilar welding and brazing of zirconium and its alloys: methods, parameters, metallurgy and properties of joints. J Manuf Process 75:928–1002. https://doi.org/10.1016/j.jmapro.2022.01.026

9. Giri SR, Khamari BK, Moharana BR (2022) Joining of titanium and stainless steel by using different welding processes: a review. Mater Today Proc 66:505–508. https://doi.org/10.1016/j.matpr.2022.05.590

10. Findik F (2011) Recent developments in explosive welding. Mater Des 32(3):1081–1093. https://doi.org/10.1016/j.matdes.2010.10.017

11. Lysak VI, Kuzmin SV (2015) Energy balance during explosive welding. J Mater Process Technol 222:356–364. https://doi.org/10.1016/j.jmatprotec.2015.03.024

12. Zhou Q, Liu R, Chen P, Zhu L (2021) Microstructure characterization and tensile shear failure mechanism of the bonding interface of explosively welded titanium-steel composite. Mater Sci Eng A 820:141559. https://doi.org/10.1016/j.msea.2021.141559

13. Wittman RH (1973) Use of explosive energy in manufacturing metallic materials of new properties. In: Proceedings of the second international symposium, Marianski Lazne, Czechoslovakia

14. Deribas AA, Simonov VA, Zakcharenko ID (1975) Investigation of explosive welding parameters for arbitrary combinations of metals and alloys. Proc sixth int conf high ener rate fab 4:1024

15. Wang Y, Li X, Wang X, Yan H (2018) Fabrication of a thick copper-stainless steel clad plate for nuclear fusion equipment by explosive welding. Fusion Eng Des 137:91–96. https://doi.org/10.1016/j.fusengdes.2018.08.017

16. Hoseini Athar MM, Tolaminejad B (2015) Weldability window and the effect of interface morphology on the properties of Al/Cu/Al laminated composites fabricated by explosive welding. Mater Des 86:516–525. https://doi.org/10.1016/j.matdes.2015.07.114

17. Inao D, Mori A, Tanaka S, Hokamoto K (2020) Explosive welding of thin aluminum plate onto magnesium alloy plate using a gelatin layer as a pressure-transmitting medium. Metals 10(1):106. https://doi.org/10.3390/met10010106

18. Akbari Mousavi SAA, Sartangi PF (2009) Experimental investigation of explosive welding of cp-titanium/AISI 304 stainless steel. Mater Des 30:459–468. https://doi.org/10.1016/j.matdes.2008.06.016

19. Shi C, Yang X, Ge Y, You J, Hou H (2017) Lower limit law of welding windows for explosive welding of dissimilar metals. J Iron Steel Res Int 24:852–857. https://doi.org/10.1016/S1006-706X(17)30126-7

20. Chen X, Inao D, Li X, Tanaka S, Li K, Hokamoto K (2022) Optimal parameters for the explosive welding of TP 270C pure titanium and SUS 821L1 duplex stainless steel. J Mater Res Technol 19:4771–4786. https://doi.org/10.1016/j.jmrt.2022.07.031

21. Tyagi T, Kumar S, Malik AK, Vashisth V (2022) A novel neuro-optimization techniques for inventory models in manufacturing sectors. JCCE 2(3):204–209. https://doi.org/10.47852/bonviewJCCE2202184

22. Wang K, Kuroda M, Chen X, Hokamoto K, Li X, Zeng X, Nie S, Wang Y (2022) Mechanical properties of explosion-welded titanium/duplex stainless steel under different energetic conditions. Metals 12(8):1354. https://doi.org/10.3390/met12081354

23. Crossland B (1982) Explosive welding of metals and its application. Clarendon Press, Oxford UK

24. Wang X (2010) Handbook of blasting. Metallurgical Industry Press, Beijing

25. Manikandan P, Hokamoto K, Deribas AA, Raghukandan K, Tomoshige R (2006) Explosive welding of titanium/stainless steel by controlling energetic conditions. Mater Trans 47:2049–2055 (https://api.semanticscholar.org/CorpusID:55280925)

26. Hokamoto K, Izuma T, Fujita M (1993) New explosive welding technique to weld aluminum alloy and stainless steel plates using a stainless steel intermediate plate. Metall Trans A 24:2289–2297. https://doi.org/10.1007/BF02648602

27. Li Z, Rostam K, Panjehpour A, Akbari M, Karimipour A, Rostami S (2020) Experimental and numerical study of temperature field and molten pool dimensions in dissimilar thickness laser welding of Ti6Al4V alloy. J Manuf Process 49:438–446. https://doi.org/10.1016/j.jmapro.2019.11.024

28. Adin MŞ (2023) A parametric study on the mechanical properties of MIG and TIG welded dissimilar steel joints. J Adhes Sci Technol 37:1–24. https://doi.org/10.1080/01694243.2023.2221391

29. Saresoja O, Kuronen A, Nordlund K (2012) Atomistic simulation of the explosion welding process. Adv Eng Mater 14(4):265–268. https://doi.org/10.1002/adem.201100211

30. Hunt JN (1968) Wave formation in explosive welding. Philos Mag 17:669–680. https://doi.org/10.1080/14786436808223020

31. Acarer M, Gülenç B, Findik F (2004) The influence of some factors on steel/steel bonding quality on there characteristics of explosive welding joints. J Mater Sci 39:6457–6466. https://doi.org/10.1023/B:JMSC.0000044883.33007.20

32. Gloc M, Wachowski M, Plocinski T, Kurzydlowski KJ (2016) Microstructural and microanalysis investigations of bond titanium grade1/low alloy steel st52-3N obtained by explosive welding. J Alloys Compd 671:446–451. https://doi.org/10.1016/j.jallcom.2016.02.120

33. Yang M, Xu J, Chen D, Ma H, Shen Z, Zhang B, Tian J (2021) Understanding interface evolution during explosive welding of silver foil and Q235 substrate through experimental observation coupled with simulation. Appl Surf Sci 566:150703. https://doi.org/10.1016/j.apsusc.2021.150703

34. Bataev IA, Lazurenko DV, Tanaka S, Hokamoto K, Bataev AA, Guo Y, Jorge AM (2017) High cooling rates and metastable phases at the interfaces of explosively welded materials. Acta Mater 135:277–289. https://doi.org/10.1016/j.actamat.2017.06.038

35. Zhang H, Jiao K, Zhang J, Liu J (2018) Microstructure and mechanical properties investigations of copper-steel composite fabricated by explosive welding. Mater Sci Eng A 731:278–287. https://doi.org/10.1016/j.msea.2018.06.051

36. Zhang B, Ma H, Xu J, Lei Li, Shen Z, Ding L, Tian J (2022) Investigations on the microstructure evolution and mechanical properties of explosive welded ODS-Cu/316 L stainless steel composite. Fusion Eng Des 179:113142. https://doi.org/10.1016/j.fusengdes.2022.113142

37. Paul H, Chulist R, Mania I (2020) Structural properties of interfacial layers in tantalum to stainless steel clad with copper interlayer produced by explosive welding. Metals 10(7):969. https://doi.org/10.3390/met10070969

38. Zhao H, Sheng L (2021) Microstructure and mechanical properties of the Ag/316L composite plate fabricated by explosive welding. J Manuf Process 64:265–275. https://doi.org/10.1016/j.jmapro.2021.01.026

39. Athar MH, Tolaminejad B (2015) Weldability window and the effect of interface morphology on the properties of Al/Cu/Al laminated composites fabricated by explosive welding. Mater Des 86:516–525. https://doi.org/10.1016/j.matdes.2015.07.114

40. Huang J, Liang G, Luo N, Li X, Chen X, Hu J (2023) Study on explosive welding A1060/3D-Printed-SUS316L. J Mater Sci Technol 27:2508–2523. https://doi.org/10.1016/j.jmrt.2023.10.096